Near-Field Far-Field Transformation in Time Domain from Optimal Plane-Polar Samples

Ovidio M. Bucci, *Fellow, IEEE*, Giuseppe D'Elia, and Marco Donald Migliore

***Abstract*— This paper presents a new approach to the time-domain near-field far-field transformation technique recently introduced by Hansen and Yaghijan [1], [2] and is based either on a time-domain or frequency-domain scheme. The approach presented here attempts to overcome the main drawbacks of this technique related to the computer time and memory requirements, which could make unrealistic the application of the technique to cases of practical interest. To this end, the advanced representation of the (time and frequency domain) near field recently introduced by the authors, which requires a minimum number of nonequispaced field samples, are exploited. This leads to new relationship between the near-field measured samples and the far field, which requires a minimal set of time–space measurements. Various computational schemes are considered and compared showing that the presented algorithm requires a reduced measurement effort, computer time, and memory occupancy, while allowing a lower far-field reconstruction error for a fixed number of measurements.**

***Index Terms*—Sampling methods, time-domain analysis.**

I. Introduction

In the last decades a large amount of work has been devoted to the characterization of radiating systems by means of near-field far-field transformation techniques. Almost all the work in this area has been carried out by considering harmonic fields so that these methods can only be used to characterize the radiated far-field at a single frequency. However, wide-band antennas for radar and telecommunication applications require the determination of the antenna performance in a wide frequency range. For these antennas, a time-domain analysis appears to be attractive since with the classical frequency domain approach a large number of measurements at different frequencies must be carried out in order to cover all the working band of the antenna under test. Furthermore, the near-field truncation error can be rigorously zero in the time-domain analysis, provided that the observation time is not too large. This new point of view has been first introduced by Hansen and Yaghijian [1]–[3].

The main problem related to the practical exploitation of this approach concerns the required amount of measured data and measurement time and, thus, the required computer time and memory storage, which can become unrealistically large for large antennas and large observation times. The number of measurements is strictly related to the available representation of the field as a function of the space–time coordinates. As a matter of fact, the existing time-domain near-field far-field (TDNF-FF) transformation techniques are based on standard (redundant) representations of the field, which, furthermore, require an unrealizable number of samples (up to infinity, in principle) when an unbounded surface is considered. Accordingly, their performances are still far from the optimal ones.

Very recently, a new optimal time-domain interpolation series has been proposed [4] for the plane-polar geometry which extend to time domain the nonredundant sampling field interpolation algorithm already introduced in the frequency domain. It allows a (numerically efficient) representation of the field with a minimum number of samples, which, furthermore, stays finite also for an unbounded observation surface. Aim of this paper is to apply these optimal interpolations of the near field for devising an effective and feasible TDNF-FF algorithm.

In Section II, two near-field far-field transformation computational schemes, based on the optimal sampling representation are introduced and discussed. The main results of an extensive numerical analysis, which show also the possibility of minimizing the size of the scanning area, are reported in Section III wherein both far-field time-signal reconstruction and frequency-domain radiation pattern evaluation are considered. Conclusions are drawn in Section IV.

II. Time-Domain Near-Field Far-Field Transformation

Let us consider a planar (nonsuperdirective) source S contained in a circle of radius a of the plane $z = -z_0$ (Fig. 1), a circular measurement region with radius R on the plane $z = 0$, and a nonharmonic radiated signal which is Fourier transformable (in the ordinary sense) and is *essentially* bandlimited to $\omega_{\max} = 2\pi c/\lambda_{\min}$[1] ($c$ is the free-space light velocity and $\lambda_{\min}$ is the wavelength corresponding to $\omega_{\max}$) with a spectrum negligible inside the interval $[-\omega_{\min}, \omega_{\min}]$ being $\omega_{\min} a/c \gg 1$.[2] A couple of coordinates $(\xi(\rho), \varphi)$ wherein (ρ, φ) are the canonical plane-polar coordinates and $\xi = \xi(\rho)$ is given in [4], (3) is considered on the measurement plane. As shown in [4], the frequency-domain field—say $\underline{E}(\xi, \varphi, \omega)$—and the time domain one—say $\underline{e}(\xi, \varphi, t)$ at $z = 0$—can be expressed by means of nonredundant interpolating

Manuscript received November 6, 1996; revised October 10, 1997.

The authors are with the Universita' di Napoli "Federico II," Dipartimento di Ingegneria Elettronica, Napoli, 80125 Italy.

Publisher Item Identifier S 0018-926X(98)05788-3.

[1] i.e., such that its spectrum outside $[-\omega_{\max}, \omega_{\max}]$ can be neglected.

[2] Due to the high-pass nature of radiating systems and to the use of pass-band signals in all applications of our interest, this assumption is always satisfied in real cases.

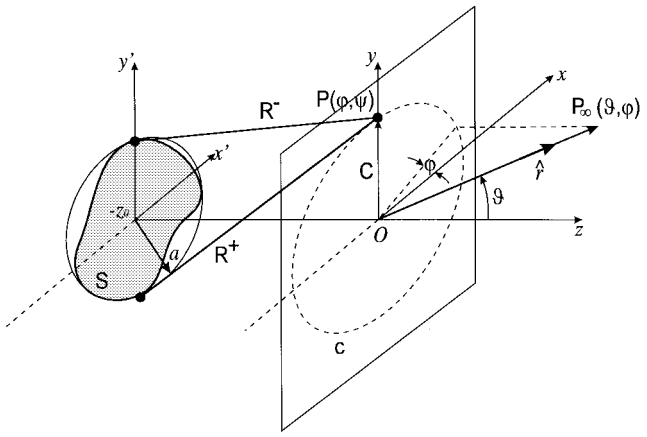

Fig. 1. Geometry of the problem.

series as

$$\underline{E}(\xi,\varphi,\omega) \cong \sum_{n=n_0-p}^{n_0+p} \sum_{m=m_0-q}^{m_0+q} \underline{E}(n\Delta\xi, m\Delta\varphi_n, \omega) \cdot e^{-j(\omega/c)(\Gamma(\xi)-\Gamma(n\Delta\xi))} \Theta_n(\varphi - m\Delta\varphi_n)\Omega(\xi - n\Delta\xi) \quad (1)$$

and

$$\underline{e}(\xi,\varphi,t) \cong \sum_{n=n_0-p}^{n_0+p} \sum_{m=m_0-q}^{m_0+q} \sum_{i=i_0-\ell}^{i_0+\ell} \underline{e}(n\Delta\xi, m\Delta\varphi_n, i\Delta t) \Theta_n(\varphi - m\Delta\varphi_n)\Omega(\xi - n\Delta\xi) \Omega\left(t - \frac{\Gamma(\xi)-\Gamma(n\Delta\xi)}{c} - i\Delta t\right) \quad (2)$$

wherein $\Delta\xi\Delta\varphi_n$, Θ_n, Ω, and $\Gamma(\xi)$ are given in [7] (central interpolation series case), Δt is given in [4], $(n_0\Delta\xi, m_0\Delta\varphi_{n_0})$ are the spatial coordinates of the sampling point nearest to the observation point (ξ,φ), $i_0\Delta t$ is the coordinate of the sampling time nearest to the observation time t, and p, q, and ℓ control the truncation error of the series (1) and (2) (typical values range between five and seven).

The frequency-domain far-field pattern in the half space $z>0$—say $\underline{\boldsymbol{\mathcal{E}}}(\vartheta,\omega)$—and the time domain one—say $\underline{f}(\vartheta,\varphi,\varphi,t)$—such that $\underline{e}(\vartheta,\varphi,r,t) = \underline{f}(\vartheta,\varphi,t-r/c)/r$ $(r\to\infty)$, are given by [1]

$$\underline{\boldsymbol{\mathcal{E}}}(\vartheta,\varphi,\omega) = -\frac{jk}{2\pi}\hat{r}\times\int_{-\infty}^{+\infty}\int_{-\infty}^{+\infty}\hat{z}\times\underline{E}(\underline{r}_0,\omega)e^{jk\underline{\hat{r}}\cdot\underline{r}_0}\,dx\,dy \quad (3)$$

and

$$\underline{f}(\vartheta,\varphi,t) = -\frac{1}{2\pi c}\hat{r}\times\hat{z}\times\int_{-\infty}^{+\infty}\int_{-\infty}^{+\infty} \cdot\frac{\partial\underline{e}(\underline{r}_0, t+\hat{r}\cdot\underline{r}_0/c)}{\partial t}\,dx_0\,dy_0 \quad (4)$$

wherein $\hat{r} = \sin\vartheta\cos\varphi\hat{x}+\sin\vartheta\sin\varphi\hat{y}+\cos\vartheta\hat{z}$ is the direction of the observation point and $\underline{r_0} = x_0\hat{x}+y_0\hat{y}$ denotes a point on the plane $z=0$.[3]

[3]It is understood that only the two tangential components of the electric field need to be measured since the z component does not contribute to integrals (3) and (4).

Due to the nonsuperdirectivity of the source and assuming $\omega_{\min}z_0/c \gg 1$, the integrals in (3) and (4) can be discretized at a $2/\lambda_{\min}$ rate by neglecting the invisible part of the field spectrum [2] so that the far-field can be expressed by means of the near-field values at all the points $\underline{r}_{0nm} = n\lambda_{\min}/2\hat{x} + m\lambda_{\min}/2\hat{y}$. For a scanning zone radius R large enough, the contribution corresponding to the indexes n,m such that $(n\lambda_{\min}/2)^2+(m\lambda_{\min}/2)^2 > R^2$ can be neglected.

Following [2], two different computational schemes can be devised for the TDNF-FF, which are based on the series obtained from (3) or (4) by discretizing the integrals and expressing the frequency- and time-domain near-field at $\underline{r}_{0nm}$ by the sampling representation (1) and (2), respectively.

Both schemes start from measurements at, say N_R points $(n\Delta\xi, m\Delta\varphi_n)$, located on a plane-polar grid covering the circular measurement region.

A. Frequency-Domain Scheme

The measurements are taken at times $t_s - t_{0nm} = s\pi/\omega_{\max}$ wherein t_{0nm} is the time of arrival of the signal at the $(n,m)_{em}$th measurement point and s range between zero and $N_t = 1+2Tf_{\max}$, T being the time interval wherein the near field is significant. The computational steps involved in this scheme follow.

1) Time-domain to frequency-domain transformation of the measured fields at N_R, points $(n\Delta\xi, m\Delta\varphi_n)$. Exploiting the fast Fourier transform (FFT), $(1/2)N_RN_t\log_2 N_t$ *complex* operations are required [2].
2) For each $\omega = 2s\omega_{\max}/N_t, s = 0,\cdots,N_t/2$,[4] a frequency-domain interpolation (1) of the samples obtained at step 1) is performed in order to evaluate the near-field on the $\pi(2R/\lambda_{\min})^2$ points $\lambda_{\min}/2$ spaced inside the measurement circle. Assuming that the sampling functions have been computed in advance, $(4R/\lambda_{\min})^2(\pi/2)pqN_t$ *complex* operations results.
3) Evaluation of the far-field $\underline{\boldsymbol{\mathcal{E}}}(\vartheta,\varphi,\omega)$ from (3) via an FFT [2]. $(4R/\lambda_{\min})^2$ points and N_t frequency are involved and $(4R/\lambda_{\min})^2(N_t/2)\log_2(4R/\lambda_{\min})$ *complex* operations are required.
4) Frequency-domain to time-domain transformation of the radiated far field by means of an inverse FFT requiring $(4R/\lambda_{\min})^2N_t/2\log_2(N_t)$ elementary operations.

When the near field is directly measured on the regular lattice of $\lambda_{\min}/2$ spaced points [2], step 1) involves all the $(4R/\lambda_{\min})^2$ points and require (1/2) $(4R/\lambda_{\min})^2N_t\log_2 N_t$ complex operations. Step 2) disappear and the steps 3) and 4) remain unchanged [2]. In all cases of practical interest, even if $N_R \ll (4R/\lambda_{\min})^2$, the additional term $(4R/\lambda_{\min})^2N_t\pi pq$ related to step 2) suggests to perform a direct measurement of the field at the regular lattice of $\lambda_{\min}/2$ spaced points.

However, it is possible to exploit a convenient computational strategy which allows to overcame this drawback. In fact, the computations required by steps 1) and 2) and involving the field data corresponding to a given sampling point can be performed *during* the measurement process, i.e., in the

[4]Because the time signal is real, only positive frequencies can be considered.

time interval occurring between the end of the data acquisition at the considered point and the start of measurements at the next point. To this end let us note that because only $2p \times 2q$ terms are involved in the summation (1), each sampling point contributes to the evaluation of only a small number of the $\lambda_{\min}/2$ spaced grid points, say $N_{n,m}$. And so, the number of complex operations required to perform the computations of step 1) and 2) and involving the considered sample is given by $N_{n,m} + (1/2)N_t \log_2 N_t$. Because $N_{n,m}$ is approximately equal to $4pq$ times the ratio between the number of points in the regular grid and the number of sampling points in the circle of radius R, i.e., $\pi(2R/\lambda_{\min})^2/N_R$, we can safely state that it is possible to perform the required computations during the time elapsing between the two successive measurements. Accordingly, taking into account that the number of required measurements N_R can be much lower than $\pi(2R/\lambda_{\min})^2$, we can say that the proposed frequency-domain computational scheme allows a substantial reduction of the measurement time without increasing the computational time. Furthermore, the memory requirements in the proposed approach are even smaller than in the standard one because we do not need to store the measured near-field values.

B. Time-Domain Scheme

Time-domain near-field to far-field transformation relies on (4) (through the discretization of the integrals) and requires the knowledge of the near-field time derivatives on a regular lattice of $\pi(2R/\lambda_{\min})^2$ points at times $t_s - t_{0nm} = s\pi/\chi_t\omega_{\max}, s = 0, \cdots, \chi_t N_t - 1, \chi_t$ being the oversampling factor that control the truncation error in the time interpolation. While in the approach adopting a plane-rectangular scanning, these values are directly measured, in our case they must be computed by means of (2), starting from the measured time-domain data at the N_R sampling points.[5] This first step requires $8pq\ell(2R/\lambda_{\min})^2 N_t \pi \chi_t$ *real* elementary operations. Then, the calculation of the far field for each observation direction $\hat{r}$ and time instant t requires first a time interpolation in order to evaluate the near field (on the regular lattice) at the times $t + \hat{r} \cdot \underline{r}_{0nm}/c$ and then the evaluation of the sum corresponding to the discretization of the integral in (4), i.e., $(2\ell + 1)\pi(2R/\lambda_{\min})^2$ operations.

In order to minimize the overall computer time, it is convenient to evaluate only the far-field samples required to cover the region of interest and then to proceed to a further sampling interpolation. Accordingly, in the extreme case of $N_R \cong \pi(2a/\lambda_{\min})^2$ far-field samples and $\pi(2R/\lambda_{\min})^2$ far-field directions, $M_t = \pi(2R/\lambda_{\min})^2 N_t \chi_t [16pq\ell + (2\ell + 1)\pi(2a/\lambda_{min})^2]$ real elementary operations are required. Since in any practical instance $8pq \ll \pi(2a/\lambda_{\min})^2$, it results in $M_t \cong (2\ell + 1)\chi_t N_t \pi^2 (2a/\lambda_{\min})^2 (2R/\lambda_{\min})^2$ so that a high-time oversampling, which allows a small value of ℓ, is highly advisable if it is compatible with memory resources. For $(2\ell + 1)\chi_t \cong 10$, we have $M_t \cong (\beta_{\max} a)^2 (\beta_{\max} R)^2 N_t$. Accordingly, this computational scheme allows a plane-polar scanning geometry with a minimum measurement effort ($N_R \leq \pi(2a/\lambda_{\min})^2$ instead of $\pi(2R/\lambda_{\min})^2$ points), with a corresponding decrease of time and memory requirements.

A much more significant increase of the overall efficiency of the measurement procedure can be obtained by again performing the required computations sequentially during the measurement process. As in the frequency-domain computational scheme, the contributions to the far field due to the time-domain near-field data corresponding to a single spatial sampling point are evaluated in the time interval occurring between two successive measurements at two successive sampling points. Taking into account that the number of measured samples to be considered for the summation with respect to the time variable is 2ℓ, that each sampling point contributes to the evaluation of the far field only through $N_{n,m}$ points $\lambda_{\min}/2$ spaced from each other, and assuming that the sampling functions have been previously evaluated and stored, the number of operations required to compute the contribution of each (spatial) sampling point to the time-domain far field at $\chi_t N_t$ times along N_R sampling directions is given by $\chi_t(2l + 1)N_{nm} N_t N_R \cong pq\ell(\beta_{\max} R)^2 \chi_t N_t$.

Again, a large oversampling turns out to be advisable.[6] Assuming that operations relative to a single sampling point can be performed in the time interval occurring between successive measurements (which is safely true in the case of not too large antennas and can be obtained, in any case, by an easy parallelization of the computational process), the only extra time is that required to evaluate the far field by sampling interpolation, which, as seen before, is proportional to $N_t(\beta_{\max} R)^2$. And so we get the significant result that, thanks to the devised computational strategy, the overall time actually required by the time-domain approach can be substantially equivalent to the frequency-domain one, thus eliminating the main drawback of the former.

Concerning the memory requirements of the technique, only the time-domain far-field (real) samples, i.e., $\chi_t N_t N_R \cong \chi_t N_t \pi(2a/\lambda_{\min})^2$ data for each far-field component, must be stored.

III. Numerical Results

In order to show the effectiveness of the presented time-domain near-field far-field transformation technique, an array of five $\hat{y}$ directed electric dipoles, placed at the edges and at the center of a square inscribed in a circle with radius $a = 120$ cm, has been considered. The dipoles are fed by a cosinusoidal current modulated by a Gaussian signal, i.e., $i(t) = e^{-4t^2/\tau^2} \cos(\omega_0 t)$. The time axis is such that the signal at the origin of the coordinate system (Fig. 1) attains its maximum at $t = 0$. Assuming that the bandwidth of the Gaussian signal is *approximately* equal to $12/2\pi\tau$ [2], the current feeding each dipole is *approximately* a pass-band

[5] As in [2], we assume that the field-time derivatives are the measured quantities. Should this not be the case, a corresponding derivative of the time-sampling functions should be inserted in series (2). It is worth noting that the exploitation of the field derivative deteriorates the signal-to-noise ratio (SNR) and is an intrinsic drawback of the approach. A careful choice of the time-domain signal should be made in order to reduce this difficulty.

[6] Note that the time interpolation can be avoided completely if a sufficiently close array of (time) near-field value is precalculated from the $\chi_t N_t$ measured values at the required (n, m) point by FFT interpolation via zero-padding, which does not increase significantly either the computer time or the memory requirements.

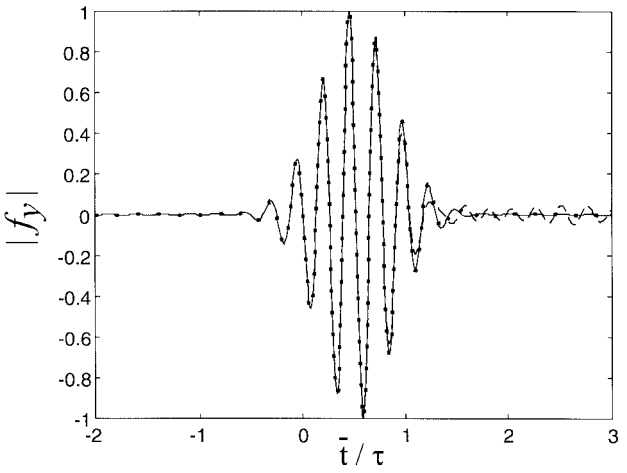

Fig. 2. Radiated far-field $\hat{y}$ component ($\vartheta = 0$). $\bar{t}$: retarded time; ——: exact signal; · · · · ·: proposed approach; − − − $\lambda_{\min}/2$ uniform near-field sampling.

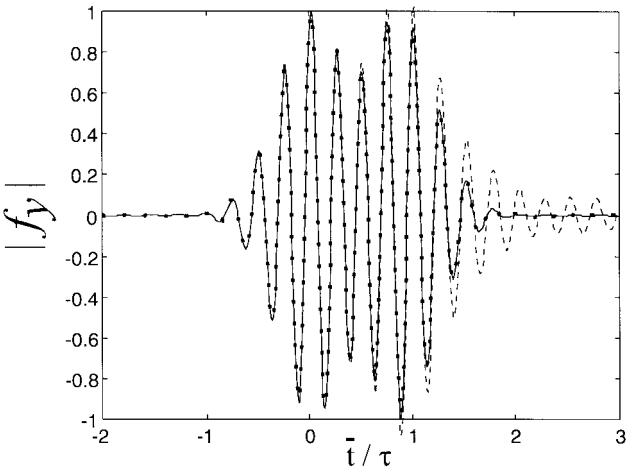

Fig. 3. Radiated far-field $\hat{y}$ component ($\vartheta = 30°, \varphi = 90°$). $\bar{t}$: retarded time; ——: exact signal; · · · · ·: proposed approach; − − − $\lambda_{\min}/2$ uniform near-field sampling.

function with $f_{\min} = f_0 - 12/2\pi\tau$ and $f_{\max} = f_0 + 12/2\pi\tau$. The numerical results reported in the following refers to $f_0 = 1$ GHz and $12/2\pi\tau = 0.5$ GHz, i.e., $f_{\min} = 0.5$ GHz, $f_{\max} = 1.5$ GHz. The circle enclosing the source has a radius $a = 6\lambda_{\min}$. The source is placed on the plane $z = -3\lambda_{\min}$.

Although the radiated field in an ideal case has an infinite time duration, in the worked examples, the signal at a point P_S on the measurement plane has been assumed *approximately* zero when the observation time t falls outside the interval $[t_{S\max} - 2\tau, t_{S\max} + 2\tau]$, $t_{S\max}$ being the time when the signal at P_S reaches its maximum.

The (spatial) sampling intervals $\Delta\xi$ and $\Delta\varphi_n$ and the number p and q were chosen in order to ensure an overall interpolation error less than -45 dB. In particular, it has been assumed $p = q = 5$ (i.e., 100 retained samples around each interpolated point) and the values of $\Delta\xi$ and $\Delta\varphi_n$ corresponding to $\chi_1 = 1.15$ and $\chi_2 = 1.3$ in [7, Tables I, II]. With these values, we get 1008 spatial sampling points distributed on 17 circumferences, the last one having radius equal to $10.56\lambda_{\min}$. The signal has been strongly oversampled in time ($\chi_t = 1.7$ corresponding to a sampling interval equal to 1.23 ps) in order to optimize the time interpolation (see Section II-B) while ensuring a completely negligible interpolation error.

As a first example, let us consider the far-field[7] $\underline{f}(\vartheta, \varphi, \bar{t})$ in the direction $\vartheta = 0$. The y component of the exact field (solid line) and the one obtained by applying the proposed approach (dotted line) are reported in Fig. 2 as function of the (normalized) retarded time $\bar{t}/\tau$. All the 1008 (space) samples have been considered and the interpolation area has been suitably increased with t in order to include all the signal. There is a good reconstruction of the signal with a maximum absolute error (normalized to the maximum absolute value of the signal) lower than -35 dB. For the sake of comparison, the far field obtained from (4) by the discretization of the integral and a direct evaluation of the near field on the regular grid of $\lambda_{\min}/2$ spaced points covering a scanning area

[7]In the following the far-field pattern $f(\vartheta, \varphi, \bar{t})$ is considered wherein $\bar{t} = t - r/c$ is the "retarded" time.

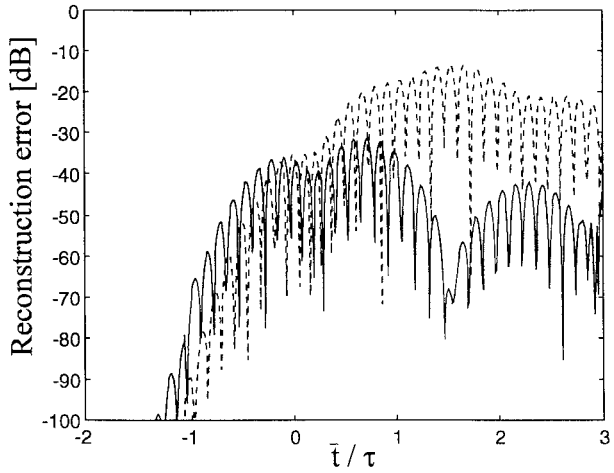

Fig. 4. Normalized error [dB] of the reconstructed far-field $\hat{y}$ component ($\vartheta = 30°, \varphi = 90°$). $\bar{t}$: retarded time, ——: proposed approach; − − − $\lambda_{\min}/2$ uniform near-field sampling.

$21\lambda_{\min} \times 21\lambda_{\min}$ wide (for a total of 1849 space samples) is shown as a dashed line in the same figure. In this case, the far-field reconstruction in essentially exact until the signal reaches the edges of the scanning area, whereas it becomes increasingly incorrect for larger observation time.

For larger observation angles, the required measurement region size increases. For the observation direction ($\vartheta = 30°, \varphi = 90°$), the exact $\hat{y}$ component of the far field (solid line), the one reconstructed by the proposed approach (dotted line), and the one calculated by directly exploiting near-field values at the regular $21\lambda_{\min} \times 21\lambda_{\min}$ lattice (dashed line) are reported in Fig. 3. Again, the proposed algorithm allows to reconstruct the field for larger $\bar{t}/\tau$ values (essentially all the signal). The reconstruction error normalized to the maximum value of the signal is reported in Fig. 4 for the presented approach (continuous line) and the standard one based on measurements on a regular grid of $\lambda_{\min}/2$ spaced points (dashed line). As can be seen, while the error of the proposed algorithm at the early times is higher, due to the interpolation error for larger value of $\bar{t}/\tau$ it is significantly lower and well behaved.

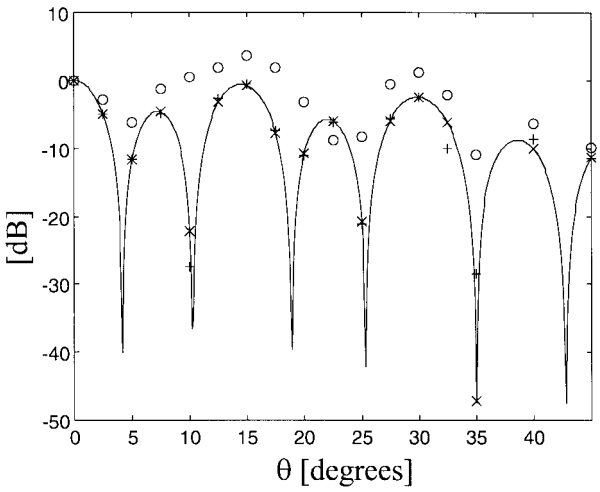

Fig. 5. Far-field pattern at $f = 627$ MHz $(0 \leq \vartheta \leq 45^\circ, \varphi = 90^\circ)$; "×": exact far-field value; "+": proposed approach ; "o": $\lambda_{\min}/2$ uniform near-field sampling.

This significant feature of the proposed approach is strictly related to the adoption of the optimal sampling expansion (2). As a matter of fact, *within the bandlimitation and truncation errors implicit in the use of (2)*, the reconstructed near field (hence, the corresponding far field) is effectively exact until the field wavefront reaches the sampling points lying outside the measurement region. As a consequence, because the radius of the circumference $\xi = n\Delta\xi$ increases rapidly with n (i.e., $\rho \to \infty$), the time required to reach the external sampling points is significantly larger for the optimal sampling than for the usual $\lambda_{\min}/2$ one. Moreover, because the neglected samples are further away from the source, the corresponding field levels are lower and the effect of truncation error is ultimately lower.

Finally, let us consider the frequency-domain radiation pattern of the antenna in the band 0.5–1.5 GHz as it is obtained by Fourier transforming the time-domain far-field signal. It must be explicitly noted that while in time domain, the error due to the finite extension of the scanning zone is essentially confined to late times; in the frequency domain, such error will affect, in principle, all the radiation pattern. Furthermore, since the proposed approach allows a better time-domain far-field reconstruction for late times (involving smaller value of the far field), it is expected that a better performance also in the frequency domain, expecially for those frequency wherein the radiated field is small (for the considered signal, occurs away from f_0). This is confirmed by Fig. 5, which shows the exact (solid line) $\hat{y}$ component of the far-field pattern, the one obtained by the proposed approach (crosses), and the one obtained by the uniform sampling approach (circles) at $f = 0.63$ GHz.

Similar results are obtained also at 1.41 GHz, whereas smaller differences between the two approaches are observed at $f = 1$ GHz (the bandwidth center), thus confirming the previous discussion.

IV. Conclusions

A new near-field far-field transformation technique in time domain based on the optimal field representations available in frequency and time domain has been presented and numerically validated. Various computational schemes have been presented and discussed both from the computational and memory requirements points of view. It results that the use of both an optimal representation of the field over the scanning plane and a proper computation strategy allows a lower number of samples, a lower overall measurement effort, a lower reconstruction error (in both time and frequency domains), and, for a given scanning area, a negligible truncation error for longer times.

References

[1] T. B. Hansen and A. D. Yaghjian, "Planar near-field scanning in the time domain—Part I: Formulation," *IEEE Trans. Antennas Propagat.*, vol. 42, pp. 1280–1291, Sept. 1994.

[2] ———, "Planar near-field scanning in the time domain—Part II: Sampling theorems and computation schemes," *IEEE Trans. Antennas Propagat.*, vol. 42, pp. 1292–1294, Sept. 1994.

[3] ———, "Formulation of probe-corrected planar near-field scanning in the time domain," *IEEE Trans. Antennas Propagat.*, vol. 43, pp. 569–584, June 1995.

[4] O. M. Bucci, G. D'Elia, and M. D. Migliore, "Optimal time-domain field interpolation from plane-polar samples," *IEEE Trans. Antennas Propagat.*, vol. 45, pp. 989–994, June 1997.

[5] O. M. Bucci, C. Gennarelli, G. Riccio, and C. Savarese, "Fast and accurate far-field evaluation from a nonredundant, finite number of plane-polar measurements," in *Proc. IEEE-APS Int. Symp.*, Seattle, WA, June 1994, pp. 540–543.

[6] ———, "Efficient Interpolation of electromagnetic fields over a cylinder from a non redundant, finite number of samples," in *Proc. PIERS Int. Symp.*, Noordwijk, The Netherlands, July 1994, pp. 1615–1619.

[7] O. M. Bucci and G. D'Elia, "Advanced sampling techniques in electromagnetics," in *Review of Radio Science 1993–1995*. New York: Oxford, 1996.

[8] O. M. Bucci and G. Franceschetti, "On the spatial bandwidth of scattered fields," *IEEE Trans. Antennas Propagat.*, vol. AP-35, pp. 1445–1455, Dec. 1987.

[9] O. M. Bucci, C. Gennarelli, and C. Savarese, "Fast and accurate near-field far-field transformation by sampling interpolation of plane-polar measurements," *IEEE Trans. Antennas Propagat.*, vol. 39, pp. 48–55, Jan. 1991.

[10] G. Di Massa and O. M. Bucci, "The truncation error in the application of sampling series to electromagnetic problems," *IEEE Trans. Antennas Propagat.*, vol. 36, pp. 941–949, July 1988.

[11] O. M. Bucci, C. Gennarelli, and C. Savarese, "Optimal interpolation of radiated field over a sphere," *IEEE Trans. Antennas Propagat.*, vol. 39, pp. 1633–1643, Nov. 1991.

Ovidio M. Bucci (SM'82–F'93), for photograph and biography, see p. 994 of the June 1997 issue of this TRANSACTIONS.

Giuseppe D'Elia, for photograph and biography, see p. 1225 of the November 1995 issue of this TRANSACTIONS.

Marco Donald Migliore, for photograph and biography, see p. 994 of the June 1997 issue of this TRANSACTIONS.